The Meteoritical Society

Meteoritics & Planetary Science 48, Nr 10, 1863–1872 (2013)
doi: 10.1111/maps.12201

Simple impact crater shape determination from shadows

J. E. CHAPPELOW

Meteorifics Inc., 1148 Sundance Loop, Fairbanks, Alaska 99709, USA
E-mail: john.chappelow@saga-inc.com

(Received 04 March 2013; revision accepted 05 August 2013)

Abstract–Crater depths, often obtained from shadow measurements, have long been used for several purposes in planetary science. However, the usual method for obtaining depth from shadow length suffers from several drawbacks and limitations. Chappelow and Sharpton (2002) introduced a much improved shadow method, which has the advantages of giving some shape information (as well as depth), and is not limited to shadows that cross the crater bottom. However, it is not general, in that it only gives very approximate crater shape information, in terms of three special cases (parabolic, conical, or flat-floored). Here, I present a completely generalized method, valid for any conic section shaped crater, and give a proof of concept and demonstration of its use, using Linne crater as a test case. In the process, I find that Linne is neither parabolic nor conical, and that it contains approximately 20 m of bottom fill, which forms a flat floor. I also conclude that the long-used parabolic paradigm for the shapes of simple craters may need to be revised.

INTRODUCTION

The diameters (D), depths (d), and shapes of impact craters have long been used for a wide variety of purposes in planetary science, including studying planetary surfaces, histories, processes, and properties. A major result of these efforts was the observation that, at smaller diameters, impact craters resemble simple, "bowl-shaped" depressions, while beyond a certain critical diameter, they are characterized by shallow, flat floors and complex features, such as central peaks and wall terraces (e.g., Melosh 2011). This critical diameter is thought to be roughly inversely related to the target body's surface gravity (Pike 1980); for Mars, the transition occurs at diameters of about 8 km (Garvin and Frawley 1998), for Mercury at about 11 km (Pike 1988), and for the Moon it is between 15 and 20 km (Pike 1980). The very simplicity of these craters provides opportunities for determining their depths and cross sectional shapes.

A particularly common, although crude, method of characterizing the shapes of simple impact craters is the depth-to-diameter ratio, d/D, which requires measurement of crater depths as well as diameters. Shadow measurements, stereogrammetry, altimetry, and photoclinometry have all been used to determine simple crater depths and morphologies (e.g., Pike 1980; Davis and Soderblom 1984; Schenk 1989; Herrick and Sharpton 2000; Garvin et al. 2011), but each of these has its own limitations. Stereogrammetry is computationally intensive, and requires at least two shadow-free images of the target crater taken from different angles, often making it difficult to apply, especially to large surface areas and to flyby imagery. Photoclinometry requires knowledge of the target surface's photometric function and can be severely affected by albedo variations, shadows, atmospheres, and integration error build up. Laser altimetry requires multiple passes over the small target crater, is also computationally intensive, and is resolution-limited by altimeter shot spacing and ground track coverage. None of these methods provide a small, accurate, easy-to-obtain-and-interpret set of parameters convenient for characterizing the cross sectional shapes of large numbers of craters, such as encountered in large-scale surveys or databases of craters.

Shadows cast in craters by the Sun have been widely used to determine their depths using the trigonometric tangent function and the simple equation $d = L/\tan\theta$ (where L is the shadow length and θ is the solar incidence angle) to calculate the elevation difference between crater rim and shadow tip (e.g.,

Arthur 1974; Pike 1980). But, this method depends upon the shadow tip landing at or very near the crater center (assumed to be the deepest point) to be accurate. In addition, this requirement can lead to serious selection effects in crater depth surveys if craters whose shadow tips do *not* lie near the crater center are systematically excluded (Chappelow and Sharpton 2002). This method also yields none of the morphological information the other three methods do, but much of which *is* contained in the shadow shape.

More recently, Chappelow and Sharpton (2002) devised a method for using shadows to determine the depths of simple craters that does not require the shadow tip to cross the crater center. Moreover, their method provides some actual cross sectional shape information, not just a depth-to-diameter ratio. In this method, the shape of the shadow is used to qualitatively determine an approximate shape for the crater—parabolic, conical, or flat-floored—and then apply an equation for the depth appropriate to one of these common craterforms, given in terms of L, θ, and D. Like any shadow method, it requires solar elevation angles sufficiently low to cast shadows, but does not require knowledge of a photometric function, acquisition of multiple images or spacecraft passes, or specific shadow lengths, and it is computationally simple and easy to apply.

But, even this method assumes that a target crater fits one of three basic shapes. Although simple craters are almost always assumed to be close to parabolic, observations of their shadows show that real craters take a variety of forms (Fig. 1), and these are not accounted for by this technique. At best, the conical and parabolic cases of Chappelow and Sharpton (2002) are just singular, special cases of what must be a continuum of conic section crater shapes. Thus, their method can give only very approximate crater shape information.

The purpose of this work is to improve upon the methods of Chappelow and Sharpton (2002) by quantitatively relating the shapes of the shadows cast within simple craters to the shapes of the craters themselves, so that crater depths and shapes may be calculated from simple measurements of these shadows. To do this, I will begin by assuming that the interior shapes of simple impact craters can be closely approximated not just by two special cases of conic sections, but by *any* conic section of revolution. These include ellipses, circles, and hyperbolas, as well as the parabolas and cones considered by Chappelow and Sharpton (2002). This assumption is motivated by several considerations:

1. The currently prevalent paradigm is that simple craters are close to parabolic (e.g., DePater and Lissauer 2001; Melosh 2011).

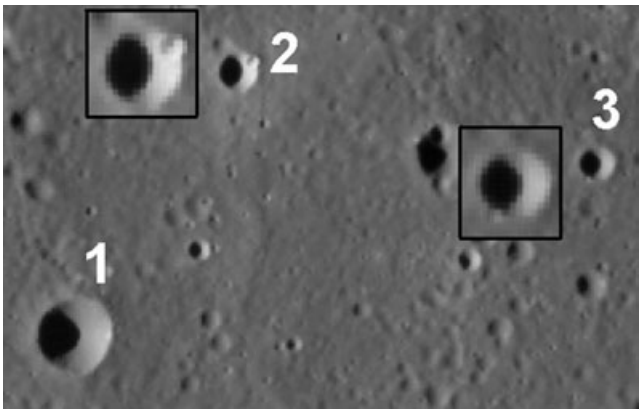

Fig. 1. A clip of a MESSENGER image of Mercury that includes several simple impact craters. All are illuminated at the same solar elevation angle (16.2°), but the variation in their shadow shapes indicates that they have quite different shapes. The highly elliptical shadowfront in crater 1 demonstrates, by inspection, that it is hyperbolic in shape. The almost circular shadowfront in crater 2 shows that it is very close to parabolic (expanded insets provided in the boxes). Crater 3's shadow indicates that it too is hyperbolic, but is an intermediate case between craters 1 and 3. (Although difficult to see in this image, crater 2 also has a bright halo of ejecta similar to Linne.)

2. The results of Chappelow and Sharpton (2002) showed that many simple craters can be reasonably approximated as either parabola-like or cone-like, and that the shapes of these two special cases can be analytically related to their cast shadows.
3. In real craters, these shadows vary considerably in shape, indicating that the crater shapes also vary significantly (Fig. 1). In fact, they imply that real simple crater shapes occupy a continuum that includes, but is not limited to, the range between cone-like and parabola-like shapes (i.e., the hyperbolas).
4. Personal observations of the shadowfronts within natural simple craters show that these shadows generally consist of smooth, circular, or elliptical arcs (Fig. 1), consistent with the results of Chappelow and Sharpton (2002).
5. Profiles of experimental (e.g., Oberbeck 1971) and natural (e.g., Ravine and Grieve 1986) craters appear, qualitatively, to have generally conic section shaped cross sections, although not necessarily parabolic ones (Fig. 2).
6. Low-velocity impact experiments by DeVet and DeBruyn (2007) that, while well outside the "hypervelocity" impact regime, resulted in craters with conic section shaped cross sections between the conical and parabolic limiting cases (i.e., they were hyperbolic).

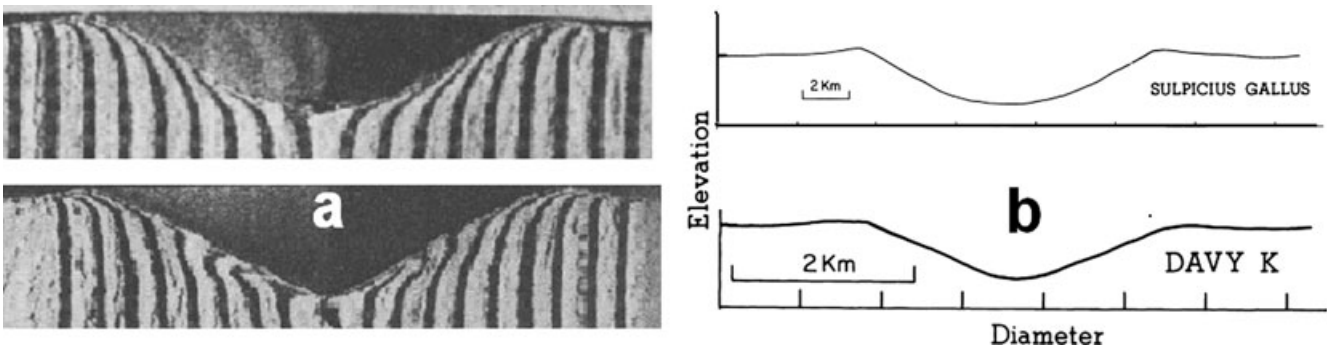

Fig. 2. Examples of conic section-like crater shapes taken from previous a) experimental and b) observational work. The upper profiles are parabola-like, while the lower profiles are cone-like. (a, adapted from Oberbeck 1971; and b, Ravine and Grieve 1986).

DERIVATION OF THE SHADOW SHAPE VERSUS CRATER SHAPE RELATIONSHIP

My first purpose here is to determine the shape of the shadow boundary, as viewed from zenith, in terms of some parameters that describe the crater shape. Consider a conic section shaped simple impact crater with radial symmetry about the vertical (z) axis, and illuminated by the Sun from above the positive x-axis by solar elevation angle ϕ (Fig. 3). The illumination source is considered distant, so its rays may be considered parallel, and the crater rim is a flat horizontal circle. The shape of the shadow cast within it is determined only by the shape of the crater's interior, and not by any rim relief, so there must be a direct relationship between the crater's shape, and the shape of the shadow cast within it. The origin of coordinates is placed at the bottom of the crater, and the y-axis forms a right-handed coordinate system with x and z.

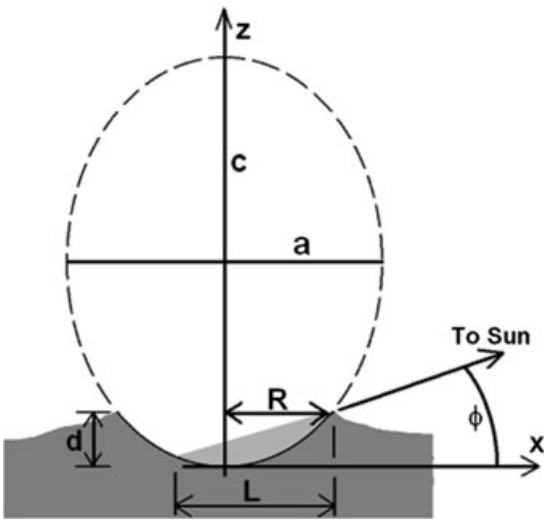

Fig. 3. A vertical cross section through the center of a crater with an elliptical cross sectional shape, illuminated at solar elevation angle ϕ above the x-axis, which casts shadow of length L. Its depth is d, radius is R, and a and c are the semiaxes of the crater shape ellipse.

Relating Crater Shape to Shadow Shape

For simplicity, in what follows I will use the case of an ellipsoidal crater shape (Fig. 3) as an example, as the geometric meanings of various quantities are clearer for this case; e.g., this is equivalent to restricting a and c to be real, positive quantities with simple meanings. However, the algebra below is completely general; it applies to all conic sections of revolution about the z-axis, which in turn correspond to other possible values for a and c (e.g., negative, imaginary, and infinite values).

So, I will begin by considering a crater whose cross section has the form of an ellipse. In z-cylindrical coordinates, the equation for the ellipsoid representing the crater is:

$$\frac{r^2}{a^2} + \frac{(z-c)^2}{c^2} = 1 \qquad (1)$$

where a and c are the radial and vertical semiaxes of the ellipsoid, respectively, which is centered at $(r, z) = (0, c)$, and with the origin of coordinates located at its bottom (Fig. 3). Because it is an ellipsoid, a^2 and c^2 must be positive numbers, and therefore a and c must be real. Furthermore, as only the lower half of the ellipsoid is of interest, c must be positive. Also, only the part of the lower half of the ellipsoid for which $z \leq d$, where d is the crater depth, represents the interior surface of the impact crater (Fig. 3). Thus, a, c, and d are three parameters that completely describe the crater's approximating conic-sectional shape.

A final quantity describing the crater is the radius, R. However, R is not an independent parameter as a, c, and d together fix R. To see why, simply evaluate (1) on

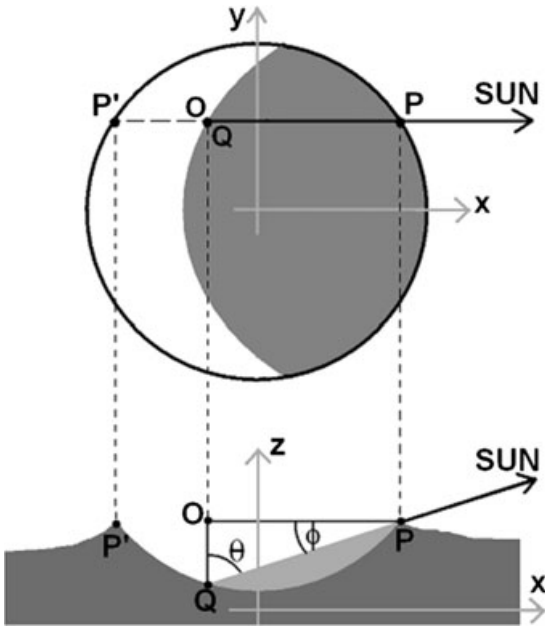

Fig. 4. A vertical cross section PP′ through a crater, parallel to the illumination direction. Plan view (top) and side view (bottom) of cross section PP′. θ is the solar incidence angle relative to the vertical. Note that the cross section is *not* through the center of the crater, but is arbitrary.

the crater rim, where $z = d$, and $r = R$. This yields the auxiliary equation:

$$\frac{R^2}{a^2} + \frac{(d-c)^2}{c^2} = 1 \tag{2}$$

which will be useful later. Thus, only three parameters—in this case a, c, and d—are sufficient to fully define the crater shape conicoid.

Next, solving (1) for z results in:

$$z = c \pm c\sqrt{1 - \frac{r^2}{a^2}} \tag{3}$$

As $z(r)$ represents a crater, we are interested here only in the lower half of the ellipsoid, which corresponds to the minus sign above, thus:

$$z = c\left(1 - \sqrt{1 - \frac{r^2}{a^2}}\right) \tag{4}$$

which relates the elevation of any point on the crater's interior surface to its radial position.

Next, consider a solar light-ray, which passes just over the crater rim at point P and is incident on the crater interior at point Q, which must, by definition, lie on the shadowfront (Fig. 4; note that these points are *not* on the shadow symmetry axis). With point O, points P and Q form a vertical right triangle OPQ, and by definition of the tangent function:

$$\tan\theta = \frac{x_P - x_O}{z_O - z_Q}. \tag{5}$$

But, $z_O = z_P = d$ and $x_O = x_Q$, and as P is on the crater rim, $x_P = +\sqrt{R^2 - y_P^2} = +\sqrt{R^2 - y_Q^2}$ (note that x_P must be positive for any point P that casts a shadow inside the crater). Substituting these for z_O, x_O, and x_P in the above equation gives:

$$\tan\theta = \frac{\left(R^2 - y_Q^2\right)^{1/2} - x_Q}{d - z_Q} \tag{6}$$

which now contains only the coordinates of the point on the shadowfront, (x_Q, y_Q, z_Q). Next, dropping the Q subscript and rearranging this to solve for z:

$$z = d - \frac{\left(R^2 - y^2\right)^{1/2} - x}{\tan\theta}. \tag{7}$$

This equation gives the elevation of any point on the shadowfront as a function of position, in rectangular coordinates. As these points must also lie on the surface of the crater, we can equate the expressions for z given by (4) and by (7):

$$d - \frac{\left(R^2 - y^2\right)^{1/2} - x}{\tan\theta} = c\left(1 - \sqrt{1 - \frac{x^2 + y^2}{a^2}}\right) \tag{8}$$

where everything is now expressed in rectangular coordinates.

Together with (2), this transcendental equation now relates the x and y coordinates of each point on the curve of the shadowfront cast inside an ellipsoidal crater, defined by a, c, and d, and illuminated at incidence angle θ. Its solutions, $y(x)$, define the boundaries of the shadow inside the crater as viewed from the zenith. While they are somewhat difficult to obtain, (8) does have two analytical solutions. The first is:

$$y = \pm\sqrt{R^2 - x^2} \tag{9}$$

(To confirm this, simply plug (9) into (8) and notice that it reduces to (2).) This solution corresponds to the rim circle of the crater, and represents the sunward boundary of the shadow.

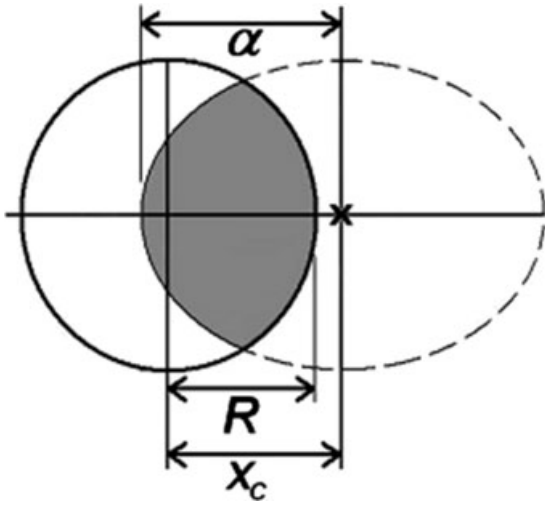

Fig. 5. Definitions of the terms that define the crater shadow bounding ellipse. Illumination is from the right, the crater's rim is the solid black circle, and it is hyperbolic in cross sectional shape. The x marks the center of the shadow boundary ellipse and is displaced by distance x_c in the direction of the Sun.

The second, much more difficult but also more interesting, solution is:

$$\frac{(x - x_C)^2}{\alpha^2} + \frac{y^2}{R^2} = 1 \tag{10}$$

where:

$$x_C = \frac{-2a^2(d - c)\tan\theta}{a^2 + c^2\tan^2\theta} \tag{10a}$$

and:

$$\alpha = \pm\left(\frac{a^2 - c^2\tan^2\theta}{a^2 + c^2\tan^2\theta}\right)R \tag{10b}$$

This second solution is the equation of an ellipse in the x–y plane, centered at $x = x_C$ and $y = 0$, and with semiaxes α in the x (illumination) direction and R in the y (transverse) direction (Fig. 5). Therefore, as viewed from the zenith, the free shadowfront in a conic section shaped crater must itself be a segment of an ellipse, and solutions (9) and (10) together define the entire boundary of the shadow.

Crater Shape as a Function of the Shadow Parameters

Thus far, Equations 2, 10a, 10b only give the shadow shape (R, α, and x_C) as functions of the crater shape (a, c, and d). But, we need the inverse, the crater shape parameters in terms of the shadow shape parameters, which are measurable/determinable from spacecraft imagery. The inversion again requires considerable algebra, but can be performed, analytically, with the following results:

$$a^2 = \left(\frac{R^2 - \alpha^2 + x_C^2}{R^2 - \alpha^2}\right)R^2 \tag{11}$$

$$a = \pm\left(\frac{R^2 - \alpha^2 + x_C^2}{R^2 - \alpha^2}\right)^{1/2}R \tag{11a}$$

$$c^2 = \left(\frac{R^2 - \alpha^2 + x_C^2}{(R - \alpha)^2\tan^2\theta}\right)R^2 \tag{12}$$

$$c = +\left(\frac{\sqrt{R^2 - \alpha^2 + x_C^2}}{(R - \alpha)\tan\theta}\right)R \tag{12a}$$

and:

$$d = \frac{\left(\sqrt{R^2 - \alpha^2 + x_c^2} - x_C\right)}{(R - \alpha)\tan\theta}R \tag{13}$$

Given measurements of R, α, and x_C from an image of a crater, calculation of a, c, and d via Equations (11–13) is sufficient to fully define the approximating conic section. Figure 6 and Table 1 qualitatively summarize the relationships between crater shapes, crater shape parameters, and shadow shape parameters. However, there are other possible choices of the crater shape parameters, and a, c, and d have certain drawbacks. First, they are rather nonintuitive except for the elliptical case; the crater shape cannot be easily visualized simply by inspection of these values (Table 1). Second, a and c grow very large for nearly parabolic craters, and are infinite (Table 1) for exactly parabolic ones (for which $\alpha = R$), which happen to fall right in the middle of our geometry-range of interest. Third, as a consequence, experience has shown that a and c can be very sensitive to even very small variations in the crater shape, and to the error inherent in doing the measurements, again especially for nearly parabolic craters. This can result in large ranges of values for a and c, even for repeated measurements of the same crater (see the section below on Linne crater). Finally, the expression for d becomes undefined (zero divided by zero) when α equals exactly R.

Fortunately, there is an alternative parameter set that largely avoids all of these difficulties. The first two of these are the crater rim diameter, D, which is obtained by direct measurement, and the eccentricity, e,

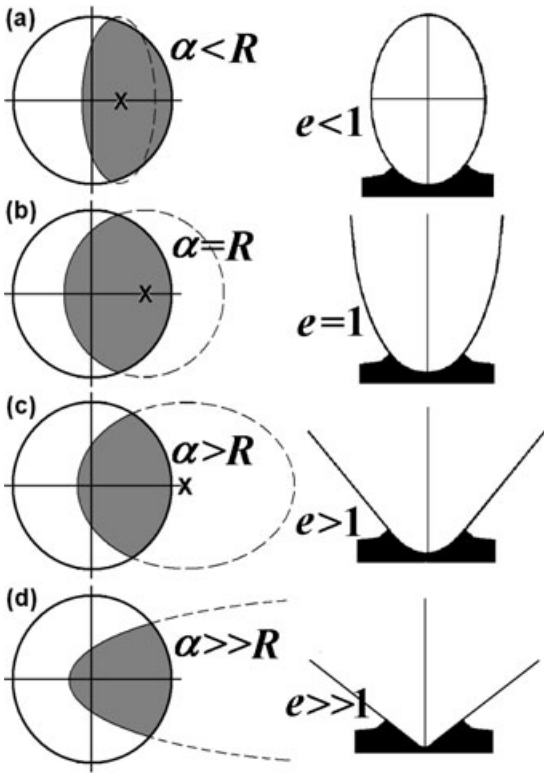

Fig. 6. Crater shadows (left) and corresponding crater shapes. a) Elliptical, b) parabolic, c) hyperbolic, and d) conical. The xs mark the centers of the shadow boundary ellipses. The singular parabolic case (b) represents the boundary between the elliptical and the hyperbolic craterforms.

of the crater shape, defined as $\sqrt{1 - a^2/c^2}$. Substituting (11) and (12) into this definition yields:

$$e = \sqrt{1 - \left(\frac{R - \alpha}{R + \alpha}\right)\tan^2\theta} \tag{14}$$

This quantity is free of singularities and varies smoothly for the conic sections of interest here. It is also readily interpretable, in terms of crater shapes and their corresponding shadow shapes: $e < 1$ for an ellipse, $e = 1$ for a parabola, and $e > 1$ for a hyperbola (Fig. 6, Table 1). As the crater shape approaches the limiting, conical case, e approaches infinity.

The third and final parameter to fix the crater shape is still the depth, d. When $\alpha = R$, Equation (13) still gives an undefined result for the depth; however, in reality, exactly parabolic craters are very rare special cases, not common ones, and in practice they are easy to recognize and handle. When this occurs, the eccentricity is, by definition, essentially equal to unity, and the depth can be calculated from the equation for the depths of exactly parabolic craters given by

Table 1. Qualitative properties of various quantities for different conic section craterforms. Note: the symbol "→" = "approaches." See Figs. 3 and 5 for graphical definitions of terms.

Crater shape	Elliptical	Parabolic	Hyperbolic	Conical
α	$<R$	$=R$	$>R$	$\rightarrow\infty$
a^2	+	$+\infty$	−	$\rightarrow-\infty$
a	± real	$+\infty$	± imaginary	$\rightarrow-\infty$ imaginary
c^2	+	$+\infty$	+	$\rightarrow 0^+$
c	+	$+\infty$	−	$\rightarrow 0^-$
e	<1	=1	>1	>>1

Chappelow and Sharpton (2002) using just the shadow length, L:

$$d = \frac{D}{4(1 - L/D)\tan\theta} = \frac{R}{(2 - L/R)\tan\theta} \tag{15}$$

The shadow length can be measured directly from the image, or calculated from: $L = \alpha - (x_c - R) = \alpha + R - x_c$ (refer to Fig. 5).

A reasonable condition for reverting to this older method is $|\alpha - R| = 0.01$, which is equivalent to defining craters within the small range $e = 1.00 \pm \sim 0.02$ to be parabolic, and to have $e = 1$.

In theory, Equations (11)–(15) constitute a means of determining the shapes and dimensions of simple craters, but is impractical to apply manually. To make use of this method, and compare it with reality, I have assembled an interactive computer program ("CRATERZ") to carry out the necessary measurements and calculations quickly and easily. After loading the image of the crater, the program reads in the image resolution and the solar azimuth and elevation, then proceeds to measurement of the crater rim and the shadow boundary ellipse. It asks the user to define the crater rim by mouse-clicking on three points on the rim, and then the shadow boundary ellipse, by clicking on two points on the free shadowfront within the crater (given other constraints, two points are sufficient to define this ellipse). These measurements can be repeated as many times as needed (I found ten trials sufficient for my purposes below), and then averaged to obtain the measured values of R, α, and x_C. From these, the program computes and outputs the crater shape parameters a, c, d, and e, using Equations (11)–(14) (Fig. 7). Along with d and D, the eccentricity, e, gives us another, independent, parameter defining the forms of craters. In the next section, I test this method against both a digital terrain model (DTM) and a laser altimeter transect of a well-known crater on the Moon.

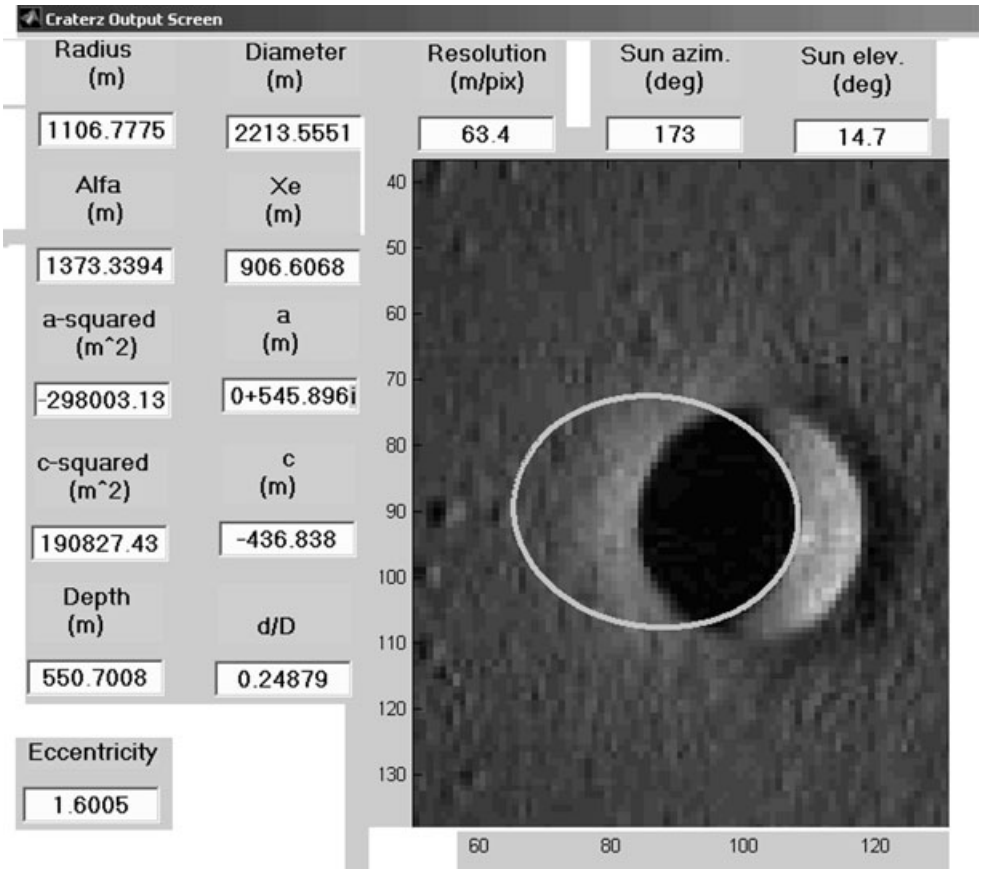

Fig. 7. A screen shot of the output screen for a typical trial of the program "CRATERZ."

PROOF OF CONCEPT—LINNE CRATER

Linne Crater is a 2.22 km diameter simple impact crater located in western Mare Serenitatis on the Moon (Fig. 8), which is noted for its bright halo of ejecta and, apparently, near-perfect "bowl shape." In fact, Linne has been widely cited as a paradigm for the entire class of features called "simple craters" (e.g., DePater and Lissauer 2001; Melosh 2011), which also implies that it has a nearly parabolic cross sectional shape (e.g., Melosh 2011). More recently, Garvin et al. (2011) concluded that Linne itself has a flat bottom, and that even its walls are not actually parabolic in shape, but instead they described it as a "truncated cone." My own observations of shadows in simple craters indicate that they vary considerably in form and that most are not parabolic, but hyperbolic in form (e.g., Fig. 1), which opens the existing, parabolic paradigm to question.

To test the shadow method, I obtained a high-resolution (2 m per pixel) digital terrain model (assembled via stereogrammetry by the Lunar Reconnaissance Orbiter Team; Garvin et al. 2011), a segment of LRO Lunar Orbiter Laser Altimeter (LOLA) data (mission elapsed time 1673100.009678 s to 1673100.973964 s), which transects very near the crater's center, and a Lunar Reconnaissance Orbiter (LRO) Wide Angle Camera (WAC) image of Linne, with appropriate illumination and viewing angles, all from the Planetary Data System (PDS). I resampled the DTM at 8 m per pixel, took 72 evenly angularly spaced (by 5°) radial cross sections of Linne from it (Fig. 9, left), and averaged them (Fig. 9, right). The LRO results show that Linne is quite radially symmetric with somewhat concave (but not parabolic) walls, and contains a small flat bottom of fallback and/or postimpact fill.

I also processed LRO_WAC image m162229369 and, for convenience, clipped out the part of the image surrounding Linne (Fig. 8). Note that this image is *not* suitable for stereogrammetry (shadows, single image), photoclinometry (shadows, albedo variations), or the traditional shadow measurement method (off-center shadow tip). In the clip, Linne is approximately 35 pixels in diameter, and the solar illumination angles are azimuth = 173° CCW from the image + x-axis, and elevation = 14.7° (θ = 75.3°). The look angle is

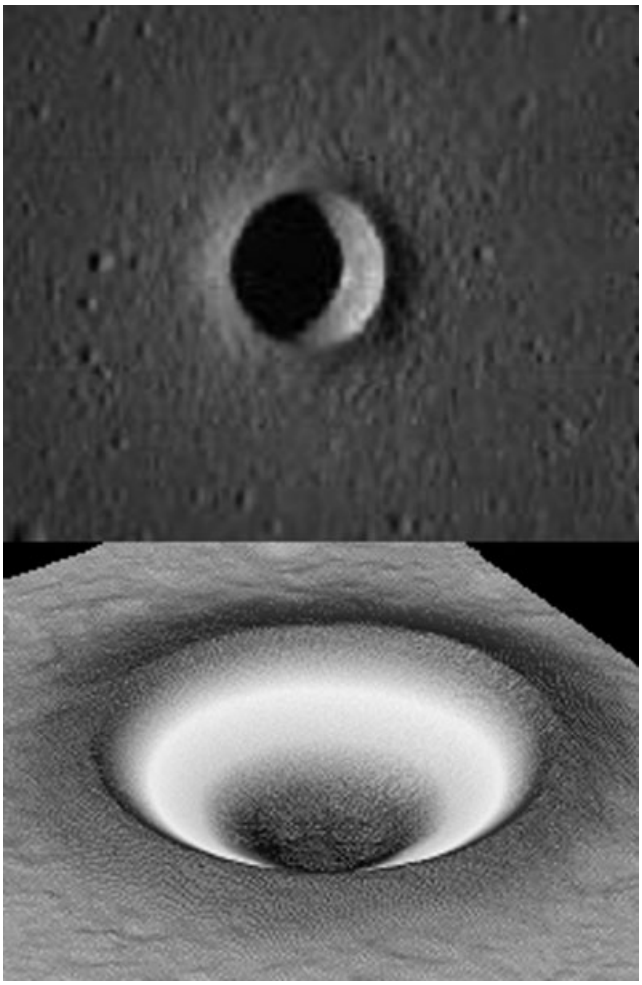

Fig. 8. Linne crater in (LRO)_ WAC image m162229369 (top) and in the grayscale-coded, 8 m pixel^{-1} resolution digital terrain model (DTM) used in this study (bottom). (DTM credit: The LRO_LROC Team.)

essentially vertical and the resolution (scale) is 63.4 m per pixel. I conducted ten trials of the measurement procedures on this image with the following results: R = 1105.2 m (σ = 10.2 m), D = 2210.5 m (σ = 20.4 m), α = 1322.5 m (σ = 87.2 m), and x_c = 855.0 m (σ = 92.9 m). Note that $\alpha > R$ indicates that Linne is hyperbolic. Calculation of the remaining crater shape parameters from these results gave d = 538.9 m and e = 1.517, and d/D = 0.244 (note that, although σ_α and σ_{xc} may seem somewhat large, d and e are, in fact, rather insensitive to this variation). This eccentricity value corresponds to a hyperbolic crater, and not a parabola *or* a cone (Fig. 6c, Table 1).

The crater shape derived above is plotted with and compared with both the DTM of Linne crater and the LOLA transect in Fig. 9. As no conic section can accurately reproduce the crater's flat bottom, the area of greatest difference is there (however, the difference between the approximating curve and the DTM profile may give a good indication of the depth of fill at the bottom of Linne: approximately 20 m). Everywhere else, the agreement between the shadow method, and the DTM and LOLA transect is excellent. Linne's flat bottom is hidden within the shadow in this case; however, whenever the flat bottoms in craters are visible, and crossed by the shadow front, they are generally easy to detect and treat (see Chappelow and Sharpton 2002), and similar estimates of bottom fill may be obtained.

Finally, personal observations indicate that, like Linne, a great majority of simple craters' shapes lie between parabolic and conical, and are therefore of the hyperbolic form rather than the elliptical. In fact, by inspection of their shadows, not a single one of the several simple craters (D > 500 m) visible in the full LRO_WAC image used above is elliptical in cross sectional shape. Thus, the widely held parabolic paradigm for simple impact craters may have to be rethought.

GUIDELINES FOR USE OF THE METHOD

Like any method, certain conditions and guidelines should or must be observed to properly apply this new shadow method. First, the derivation, and analytic solutions, of the equations on which this method is based depend upon the symmetries offered by the assumed nadir-looking viewing geometry, and the approximate symmetry and circularity of the subject craters. Therefore, the method should be limited to near nadir-looking ($\theta \leq \sim 2°$) imagery of craters on relatively flat terrain, and should not be applied to craters with significantly noncircular rims or irregular shadowfronts. Care must also be taken when applying the method to map-projected imagery, as map projection involves distorting a curved planetary surface, and all of its features (including circular impact craters), into a flat one. For example, the common equi-rectangular projection, which works with little distortion at low- to midlatitudes, tends to deform the surface substantially at higher latitudes, stretching circular features into east–west ellipses. This is not often a significant problem and is generally easy to detect when it does occur (e.g., attempting to fit the rims of the craters with circles will fail); however, users must be aware of the possibility to avoid it.

Second, although this method does not require the shadowfront to pass through the crater center, ideally, the shadowfront still must reach as deeply into the crater as possible. For any depths that the shadowfront (not the shadow proper) does not reach, the method essentially extrapolates the shape from the crater shape

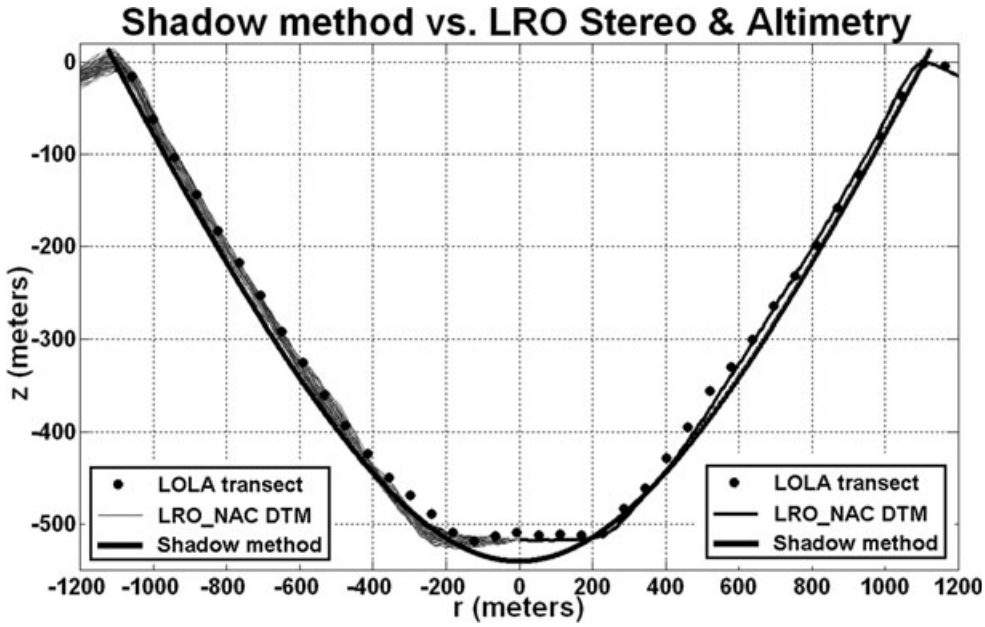

Fig. 9. Comparison of Linne crater shapes obtained via LRO_NAC stereogrammetry, LRO_LOLA laser altimetry, and the shadow measurement method described herein. The 72 individual radial profiles taken from the DTM are shown on the left and their average on the right. The section is vertically exaggerated by a factor of approximately 2.5.

and shadow shape higher on the walls. For example, in the measurement of Linne above, the crater's flat bottom lies just within the shadowfront, and is therefore hidden within the shadow. Requiring the shadowfront to pass within the middle half (i.e., $0.25D < L < 0.75D$) of the crater ensures that the shadowfront reaches to at least half the crater depth, in an exactly conical crater, and considerably deeper in the much more common (hyperbolic and elliptical) crater types.

I have also found through experience that placement of the rim points, and especially the shadowfront points, is also important. To minimize error, the three rim points should be selected as far apart as possible—ideally 120° apart. One point on the shadowfront should be selected as near the shadow tip as possible, the other as near the rim as possible, but on opposite sides of the illumination (x) axis and not exactly upon it. They should not be placed symmetrically about the illumination axis, as this leads to an insoluble set of equations for the shadow ellipse. These placements minimize the sensitivity of R, α, and x_C to small errors in point selection.

Of course, even with ideal placement, random (measurement) error in the exact positioning of the rim points, and especially the shadowfront points, will still result in some error in the shadow shape quantities derived from them (R, α, and x_C). Thus, repeated measurements of the shadow boundary ellipse can result in values of α and x_C with significant scatter (see the results for Linne crater above). This effect arises because only part of the shadow boundary ellipse is physically present—in cases of craters approaching conical in shape only a small part of the shadow boundary ellipse may be visible (Fig. 6d). This tends to magnify the measurement error; therefore, it is important to do multiple trials of at least the shadow ellipse measurement, and to inspect the fit and the scatter of the results. Through trial and error I found that, for the case of Linne presented above, 10 trials were more than sufficient to obtain the excellent fit shown in Fig. 9. For craters more conical in shape than Linne, more trials may be needed, while for more parabola-like craters, only one might be necessary. However, I have also found that the actual, physical quantities sought after (d and e) are not very sensitive to the error in α and x_C (again, see above on Linne).

Finally, subject to these guidelines, this method should be applicable to any simple crater, from meters to kilometers in diameter, given appropriate imagery. However, I do not recommend application of this method to craters less than approximately 12 pixels across. Even below $D = \sim 20$ pixels, the rim, and especially the shadowfront, often becomes noticeably indistinct, and at $D = \sim 10$ pixels, results become essentially meaningless due to an inability to adequately define the free shadowfront.

Undoubtedly, as this method gets more use and testing, these guidelines will be refined.

CONCLUSIONS

In this work, I have described and demonstrated a new method for determining shapes and dimensions of simple impact craters that will greatly enhance the usefulness of shadow measurement in general, in terms of both applicability and productivity. It can be used in situations where the other complementary methods (stereogrammetry, photoclinometry, altimetry) would be impractical or impossible to apply; is fast and easy to use; and yields simple, easy-to-interpret results. It also yields more precise depths, as well as accurate crater shape information (Fig. 9) inaccessible to previous shadow techniques, and can do so for relatively large numbers of craters. Indeed, it allows for the semiquantitative estimation of crater shapes simply by inspection of their shadows (Fig. 1). The capabilities enabled by this new shadow method will undoubtedly be useful in the future, for such tasks as determining the relative ages of impact craters, quantifying and comparing their "preservation states," deducing their provenance (e.g., primary versus secondary), and as indicators of surface processes, for example.

In the process of comparing this new method with a high-resolution DTM and a LOLA transect, it has been shown that Linne Crater is neither parabolic, as often assumed, nor in fact conical, but instead intermediate between the two: it is hyperbolic. Furthermore, this is probably true of a majority of simple craters on the Moon and other bodies, and therefore the ideal of the parabolic simple crater may need to be re-evaluated.

Acknowledgments—The author thanks reviewers V. V. Svetsov and M. Zanetti for their efforts and helpful comments, which undoubtedly improved the quality of this manuscript. This work is dedicated to the memory of R. E. Chappelow, who provided many thoughtful comments and criticisms in the development of this shadow method.

Editorial Handling—Dr. Natalia Artemieva

REFERENCES

Arthur D. W. G. 1974. Lunar crater depths from Orbiter IV long focus photographs. *Icarus* 23:116–122.

Chappelow J. E. and Sharpton V. L. 2002. An improved shadow measurement technique for constraining the morphology of simple impact craters. *Meteoritics & Planetary Science* 37:479–486.

Davis P. A. and Soderblom L. A. 1984. Modeling crater topography and albedo from monoscopic Viking Orbiter images: 1. Methodology. *Journal of Geophysical Research*. 89:9449–9457.

DePater I. and Lissauer J. J. 2001. *Planetary sciences*. New York: Cambridge University Press.

DeVet S. J. and DeBruyn J. R. 2007. Shape of impact craters in granular media. *Physical Review E* 76:041306, doi:10.1103/PhysRevE.76.041306.

Garvin J. B. and Frawley J. J. 1998. Geometric properties of Martian impact craters: Preliminary results from the Mars Orbiter Laser Altimeter. *Geophysical Research Letters* 25:4405–4408.

Garvin J. B., Robinson M. S., Frawley J., Tran T., Mazarico E., and Neumann G. 2011. Linne: Simple lunar mare crater geometry from LRO observations (abstract #2063). 42nd Lunar and Planetary Science Conference. CD-ROM.

Herrick R. R. and Sharpton V. L. 2000. Implications from stereo derived topography of Venusian impact craters. *Journal of Geophysical Research* 105E:20245–20262.

Melosh H. J. 2011. *Planetary surface processes*. New York: Cambridge University Press.

Oberbeck V. R. 1971. Laboratory simulation of impact cratering with high explosives. *Journal of Geophysical Research* 76:5732–5749.

Pike R. J. 1980. Control of crater morphology by gravity and target type: Mars, Earth, Moon. Proceedings, 11th Lunar Planetary Science Conference. pp. 2159–2189.

Pike R. J. 1988. Geomorphology of impact craters on Mercury. In *Mercury*, edited by Vilas F., Chapman C. R., and Matthews M. S. Tucson, Arizona: University of Arizona Press. pp. 165–273.

Ravine M. A. and Grieve R. A.F. 1986. An analysis of morphologic variation in simple lunar craters. *Journal of Geophysical Research* 91:E75–E83.

Schenk P. M. 1989. Crater formation and modification on the icy satellites of Uranus and Saturn: Depth/diameter and central peak occurrence. *Journal of Geophysical Research* 94:3813–3832.